A global 5km monthly potential evapotranspiration dataset (1982–2015) estimated by the Shuttleworth-Wallace model

Shanlei Sun[1], Zaoyin Bi[1], Jingfeng Xiao[2], Yi Liu[3], Ge Sun[4], Weimin Ju[5], Chunwei Liu[6], Mengyuan Mu[7], Jinjian Li[8], Yang Zhou[1], Xiaoyuan Li[1], Yibo Liu[6], Haishan Chen[1]

[1]Collaborative Innovation Center on Forecast and Evaluation of Meteorological Disasters/Key Laboratory of Meteorological Disaster, Ministry of Education/International Joint Research Laboratory on Climate and Environment Change, Nanjing University of Information Science and Technology, Nanjing, China

[2]Earth Systems Research Center, Institute for the Study of Earth, Oceans, and Space, University of New Hampshire, Durham, USA

[3]School of Civil and Environmental Engineering, University of New South Wales, Sydney, Australia

[4]Eastern Forest Environmental Threat Assessment Center, Southern Research Station, USDA Forest Service, Raleigh, USA

[5]International Institute for Earth System Science, Nanjing University, Nanjing, China

[6]Jiangsu Key Laboratory of Agricultural Meteorology, School of Applied Meteorology, Nanjing University of Information Science and Technology, Nanjing, China

[7]ARC Centre of Excellence for Climate Extremes and Climate Change Research Centre, University of New South Wales, Sydney, Australia

[8]School of Atmospheric Sciences/Plateau Atmosphere and Environment Key Laboratory of Sichuan Province, Chengdu University of Information Technology, Chengdu, China

Correspondence to: Shanlei Sun (sun.s@nuist.edu.cn)

Contents of this file

Introduction

In Text S1–3, computations for net radiation, vapour deficit pressure and soil heat flux are shown. Text S4 provides computations for aerodynamic resistance and soil boundary layer resistance, while the computations for vegetation boundary layer resistance and soil surface resistance are presented in Text S5 and S6, respectively. Figures S1 depict monthly validation result for net shortwave radiation estimated based on the CERES satellite-based observations and the CRU TS4.06 cloud cover data. Spatial distribution of the reconstructed canopy height across the globe is illustrated in Figure S2, while Figure S3 shows validation results for the calibrated SW model by the observations at all of 96 sites. Table S1 presents basic information of the used 96 EC sites for calibrating the SW model in this study, while typical height for the 5 CSCS-based GRA groups and cropland height are shown in Tables S2 and S3, respectively. In Table S4, the w, z_{0g} and α_m values for various LULC types are given. The calibrated values of r_{smin} for each LULC type is presented in Table S5.

Text S1 Computation for net radiation (R_n)

The MSWX-Past R_n

For comprehensively utilizing radiation variables [e.g., downward shortwave radiation (R_{ds}, W/m^2), and downward longwave radiation (R_{dl}, W/m^2)], the MSWX-Past R_n (W/m^2) can be expressed as:

$$\begin{cases} R_n = (1-\alpha)R_{ds} + R_{nl} & \text{(S1a)} \\ \alpha = \alpha_m - (\alpha_m - \alpha_s)\exp(-0.56LAI) & \text{(S1b)} \\ R_{nl} = \varepsilon R_{dl} - \varepsilon \dfrac{5.67}{100000000}(T_{mean}+273.16)^4 & \text{(S1c)} \end{cases}$$

where α is land surface albedo (unitless), which is related to the albedo of the "closed" canopy (i.e., α_m, unitless) and the bare soil (α_s, unitless; Uchijima, 1976); R_{nl} is net longwave radiation (W/m^2); T_{mean} is mean air temperature at 2 m height (^{o}C); ε denotes land surface emissivity (unitless). Considering the major focus of PET in this study, α_s is set to 0.1 to represent the albedo of the wet bare soil (Shuttleworth, 1993). α_m is collected from the literature and varies among land use/land cover (LULC) types (Table S1; Zhou et al., 2006).

The ERA5 and MERRA-2 R_n

The ERA5 and MERRA-2 provide net shortwave radiation (R_{ns}, W/m^2) and R_{nl}, and therefore the corresponding R_n can be obtained using the equation below:

$$R_n = R_{ns} + R_{nl} \quad \text{(S2)}$$

The CRU TS4.06 R_n

Due to lack of R_{ds} within the CRU TS4.06, the CERES satellite-based R_{ds} will be used to estimate the1982–2015 R_{ds} time series based on the physical relationship between R_{ds} and cloud cover (*Cld*, unitless). In this study, the cloud-based R_{ds} algorithm of Reddy (1974) is used, and the major equations and the detailed procedures are shown below.

$$\begin{cases} R_{ds} = [a_s + b_s(1-Cld)]R_e & \text{(S3a)} \\ R_e = \dfrac{1666.67}{\pi} G_{sc} d_r [\omega_s \sin(\phi)\sin(\delta) + \cos(\phi)\cos(\delta)\sin(\omega_s)] & \text{(S3b)} \\ dr = 1 + 0.033\cos(\dfrac{2\pi}{365}J) & \text{(S3c)} \\ \delta = 0.0409\sin(\dfrac{2\pi}{365}J - 1.39) & \text{(S3d)} \\ R_{nl} = \sigma \dfrac{T_{min,K}^4 + T_{max,K}^4}{2}\left[0.34 - 0.14\sqrt{ea}\right]\left(1.35\dfrac{R_{ds}}{R_{s0}} - 0.35\right) & \text{(S3e)} \\ R_{s0} = (a_s + b_s)R_e & \text{(S3f)} \end{cases}$$

where R_e (W/m^2) and G_{sc} (= 1366.67 W/m^2) are extraterrestrial radiation and solar constant, respectively; d_r denotes inverse relative distance Earth-Sun; ω_s (rad), φ (rad) and δ (rad) denotes sunset hour angle, latitude and solar decimation of a given weather site, respectively; J represents the number of the day in the year between 1 (i.e., 1 January) and 365 or 366 (i.e., 31 December); a_s is regression constant, expressing the fraction of R_e reaching the Earth on overcast days (i.e., *Cld*=1); and a_s+b_s represents fraction of R_e reaching the earth on clear days (i.e., *Cld*=0); σ is Stefan-Boltzmann constant; $T_{max,K}$ (K) and $T_{min,K}$

(K) denote maximum and minimum absolute temperature, respectively.

Despite that the reference values for a_s (=0.25) and b_s (=0.50) are given in Allen et al. (1998), their spatio-temporal differences may impact the accuracy of the estimated R_{ds}. Thus, we firstly resampled the CERES R_{ds} into $0.5^o \times 0.5^o$ for meeting the CRU TS4.06 *Cld* resolution, and used the linear regression to fit a_s and b_s of EQ. S6a in each month at each CRU TS4.06 grid with the CERES R_{ds} and the *Cld* in 2001–2015 and the least square method. Subsequently, these coefficients were be employed to calculate monthly R_{ds} at each grid during 1982–2015 based on the CRU *Cld* data. In this study, we would like to follow the computation procedures from Allen et al. (1998) to calculate R_{nl} (i.e. EQs. S6e and S6f). At last, R_n can be calculated based on EQ. S4a.

Text S2 Computation for vapour deficit pressure (*D*)

The MSWX-Past *D*

$$\begin{cases} e_s = \dfrac{0.6108\exp\left(\dfrac{17.27T_{max}}{237.3+T_{max}}\right) + 0.6108\exp\left(\dfrac{17.27T_{min}}{237.3+T_{min}}\right)}{2} & \text{(S4a)} \\ D = e_s(1-Rh) & \text{(S4b)} \end{cases}$$

where e_s is the saturated vapour pressure (kPa); Rh is the relative humidity (%); T_{min} and T_{max} is the minimum and maximum air temperatures (°C).

The CRU TS4.06 *D*

$$D = e_s - e_a \quad \text{(S5)}$$

where e_s is estimated based on EQ. S7a and the CRU TS4.06 minimum and maximum air temperatures; e_a is the actual vapour pressure (kPa).

The ERA-5 D

$$D = e_s - 0.6108\exp\left(\frac{17.27d_{2m}}{237.3+d_{2m}}\right) \quad \text{(S6)}$$

where e_s is estimated based on EQ. S7a and the ERA-5 minimum and maximum air temperatures; d_{2m} is the dewpoint temperature (°C).

The MERRA-2 D

$$D = e_s - Pres\frac{Sh}{0.622} \quad \text{(S7)}$$

where e_s is estimated based on EQ. S7a and the MERRA-2 minimum and maximum air temperatures; *Pres* is the atmospheric pressure (kPa); *Sh* is the specific humidity (kg/kg).

Text S3 Computation for soil heat flux (*G*)

The soil heat flux (G, W/m^2) is computed according to the equation of Allen et al. (1998):

$$G = 0.81\left(T_{mean,+1} - T_{mean,-1}\right) \quad \text{(S8)}$$

where $T_{mean,-1}$ and $T_{mean,+1}$ are the mean air temperatures in pervious and next months (°C), respectively.

Text S4 Computations for aerodynamic resistance (r_a^a) and soil boundary layer resistance (r_a^s)

In this study, the formulation of Shuttleworth and Gurney (1990) is used to compute r_a^a and r_a^s. Their equations are shown as:

$$\begin{cases} r_a^a = \dfrac{1}{ku_*}\ln\left(\dfrac{z_a - d_0}{h - d_0}\right) + \dfrac{h}{nK_h}\left\{\exp\left[n\dfrac{1-(Z_0+d_p)}{h}\right] - 1\right\} & \text{(S9a)} \\ r_a^s = \dfrac{h\exp(n)}{nK_h} \times \left\{\exp\left(-\dfrac{nz_{0g}}{h}\right) - \exp\left[-\dfrac{n(Z_0+d_p)}{h}\right]\right\} & \text{(S9b)} \end{cases}$$

where h is the vegetation height (m); n is the eddy diffusivity decay constant of the vegetation (unitless); K_h is the eddy diffusion coefficient at the top of canopy (m^2/s); z_{0g} indicates the roughness length of ground (m), and varies with the vegetation type (Table S1); Z_0 is the "preferred" roughness length (m), equaling to $0.13h$; d_p denotes the "preferred" zero plane displacement (m), and is set to $0.63h$; k (= 0.41) is von Karman's constant; u_* is the friction velocity (m/s); z_a is the reference height (m) and equals to $2+h$; d_0 is the zero plane displacement of canopy (m). All terms within EQ. S1 are parameterized according to Monteith (1973), Choudhury and Monteith (1988), Shuttleworth and Gurney (1990), Federer et al. (1996), and Allen et al. (1998), such as,

$$\begin{cases} K_h = ku_*(h - d_0) & \text{(S10a)} \\ u_* = ku_a / \ln\left[\dfrac{z_a - d_0}{z_0}\right] & \text{(S10b)} \\ u_a = u_m \dfrac{\ln(67.8z_a - 5.42)}{\ln(67.8h_m - 5.42)} & \text{(S10c)} \\ d_0 = \begin{cases} h - z_{0c}/0.3, & \text{(Closed camopy: LAI} \geq 4\text{)} \\ 1.1h\ln[1 + (c_d\text{LAI})^{0.25}], & \text{(Sparse growing vegetation: LAI} < 4\text{)} \end{cases} & \text{(S10d)} \\ z_0 = \min\left[0.3(h - d_0),\quad z_{0g} + 0.3h(c_d\text{LAI})^{0.5}\right] & \text{(S10e)} \\ z_{0c} = \begin{cases} 0.13h, & \text{Short vegetation: } h \leq 1 \\ 0.05h, & \text{Tall vegetation: } h \geq 10 \\ 0.139h - 0.009h^2, & \text{Others: } 1 < h < 10 \end{cases} & \text{(S10f)} \\ c_d = \begin{cases} 1.4 \times 10^{-3}, & h = 0 \\ [-1 + \exp(0.909 - 3.03z_{0c}/h)]^4/4, & h > 0 \end{cases} & \text{(S10g)} \\ n = \begin{cases} 2.5, & \text{Short vegetation: } h \leq 1 \\ 4.25, & \text{Tall vegetation: } h \geq 10 \\ 2.306 + 0.194h, & \text{Others: } 1 < h < 10 \end{cases} & \text{(S10h)} \end{cases}$$

where u_a and u_m represent the wind speed at the reference height and the height of measurement above ground surface, respectively (m/s); h_m is the height of measurement above ground surface (m); z_0 is the roughness length of canopy (m), however z_{0c} is that for a "closed" canopy (m); c_d is the mean drag coefficient for individual leaves (unitless).

Text S5 Computation for vegetation boundary layer resistance (r_a^c)

According to Shuttleworth and Wallace (1985), Shuttleworth and Gurney (1990), and Brisson et al. (1998), all leaf boundary layers are in parallel and then the r_a^c can be expressed as:

$$\begin{cases} r_a^c = \dfrac{\left(\dfrac{100}{n}\right)\left(\dfrac{w}{u_h}\right)^{\frac{1}{2}}\left[1-\exp\left(-\dfrac{n}{2}\right)\right]^{-1}}{2\mathrm{LAI}} & \text{(S11a)} \\ w = \begin{cases} w_{max}, & for\ perennial\ vegetation \\ w_{max}[1-\exp(-0.6\mathrm{LAI})] & for\ annual\ vegetation \end{cases} & \text{(S11b)} \end{cases}$$

where w denotes canopy characteristic leaf width (m), while w_{max} is maximum vegetation leaf width (m; Table S1); u_h is the wind speed at the top of canopy (m/s).

Text S6 Computation for soil surface resistance (r_s^s)

In this study, the parameter of r_s^s is estimated based on Villagarcía et al. (2010), and can be written as:

$$r_s^s = x\theta_{sat}^y \quad \text{(S12)}$$

where θ_{sat} is saturated water content in soil (cm^3/cm^3), while x and y are the fitting coefficients for this equation. Considering differences in r_s^s under different vegetation coverage conditions, the coefficients of x (y) are set to 111.86 (-0.58) for plant position but 36.821 (-1.42) for bare soil position. The global θ_{sat} at the first soil layer (i.e., 0–0.0451 m) is used here, and collected from http://globalchange.bnu.edu.cn/research/soil5.jsp (Dai et al., 2019a, 2019b).

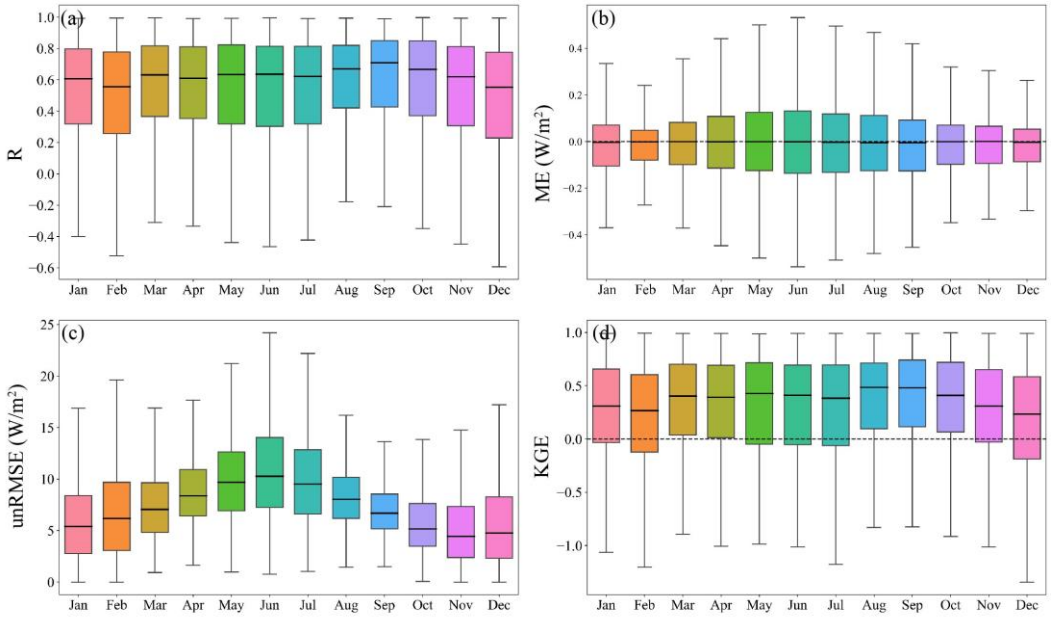

Figure S1: Monthly validation result for net shortwave radiation estimated based on the CERES satellite-based observations and the CRU TS4.06 cloud cover data.

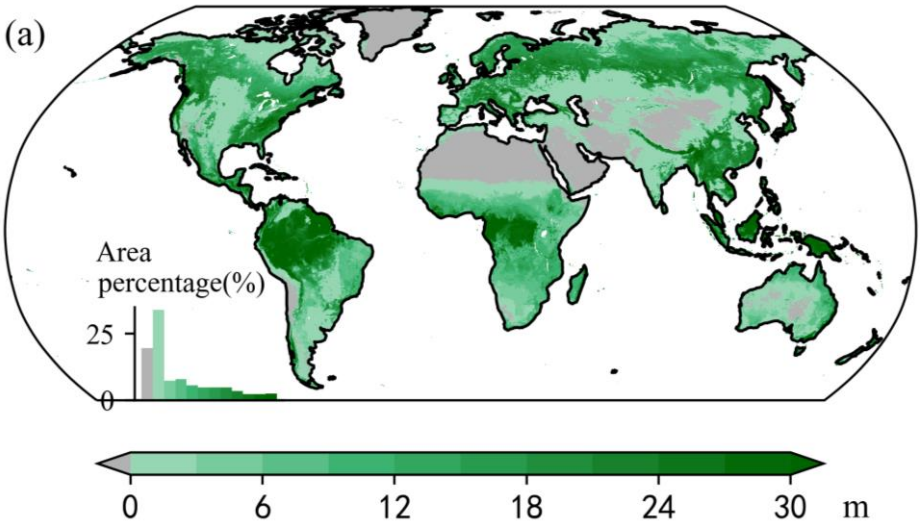

Figure S2: Spatial distribution of the reconstructed canopy height across the globe.

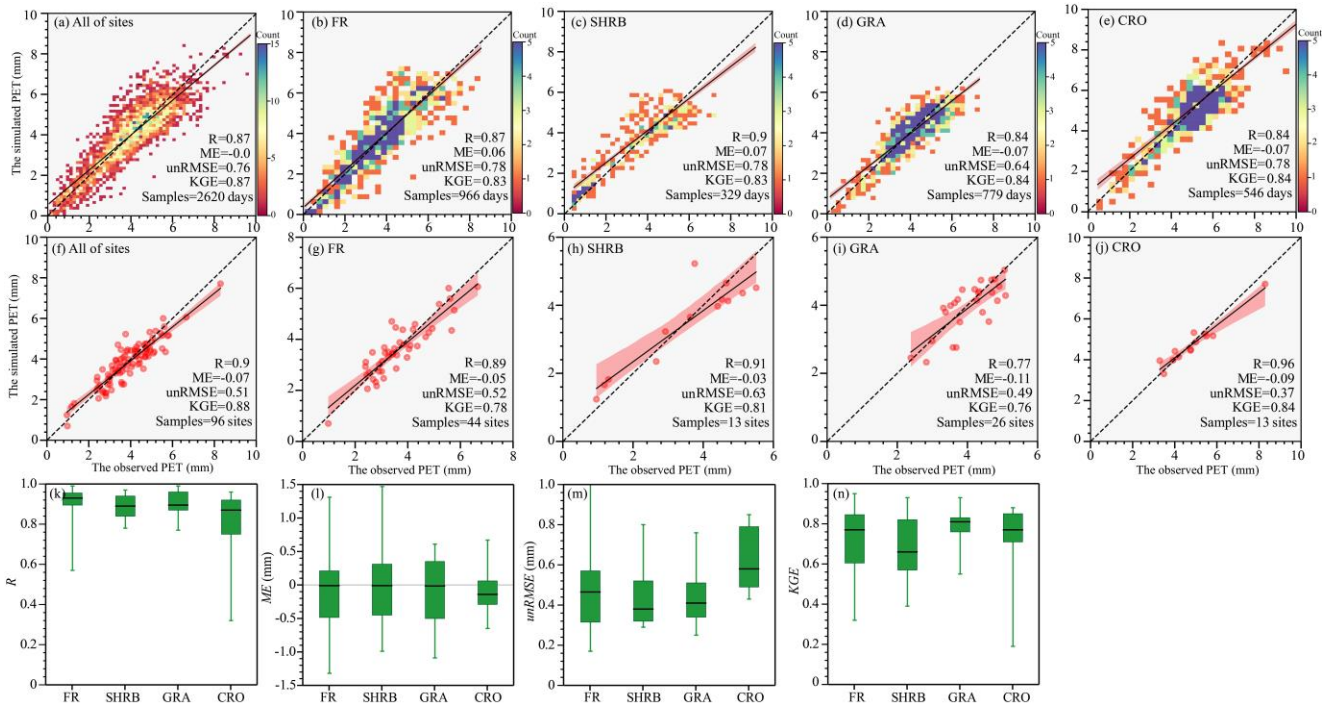

Figure S3: Validation results for the calibrated SW model by the observations at all of 96 sites. (a): Comparison for daily PET at all of 96 sites. (b-e): Comparison for daily PET for each LULC. (f): Comparison for site mean PET at all of 96 sites. (g-j): Comparison site mean PET for each LULC. (k-n) Boxplots of the validation metrics of daily PET simulations for each LULC. The whiskers represent the minimum and maximum values of the model performance metrics. The outer edges of the boxes and the horizontal lines within the boxes indicate the 25th, 75th, and 50th percentiles of the validation metrics.

Table S1: Basic information of the used 96 EC sites for calibrating the SW model in this study

IGBP LULC type	Names	Latitude (°)	Logtitude (°)	Altitude (m)	Country	Date	Unstressed days
	US-SP1[a,]	29.74	-82.22	50	USA	2005/1/1—12/31	8
	US-SP2[a]	29.76	-82.24	50	USA	2000/1/1—2004/12/31	38
	CA-Qcu[a]	49.27	-74.04	392	Canada	2002/1/1—2006/12/31	8
	DE-Bay[a]	50.14	11.87	/	Germany	1997/1/1—1999/12/31	11
	DE-Lkb[b,e]	49.10	13.30	1308	Germany	2009/1/1—2013/12/31	8
	CA-SF2[b,e]	54.25	-105.88	536	Canada	2001/1/1—2005/12/31	13
	CA-SF1[b,e]	54.49	-105.82	520	Canada	2003/1/1—2006/12/31	13
	FI-Hyy[b,e]	61.85	24.29	181	Finland	1996/1/1—2014/12/31	11
	IT-SRo[b,e]	43.73	10.28	6	Italy	1999/1/1—2012/12/31	18
Evergreen	IT-Ren[b,e]	46.59	11.43	1730	Italy	1998/1/1—2013/12/31	14
Needle Forest	DE-Obe[b,e]	50.79	13.72	735	Germany	2008/1/1—2014/12/31	13
(ENF)	CA-TP1[b,e]	42.66	-80.56	265	Canada	2002/1/1—2014/12/31	27
	CA-Qfo[b,e]	49.69	-74.34	382	Canada	2003/1/1—2010/12/31	18
	RU-Fyo[b,e]	56.46	32.92	265	Russia	1998/1/1—2014/12/31	16
	IT-Lav[b,e]	45.96	11.28	1353	Italy	2003/1/1—2014/12/31	31
	US-Blo[b,e]	38.90	-120.63	1315	USA	1997/1/1—2007/12/31	46
	NL-Loo[b,e]	52.17	5.74	25	The Netherlands	1996/1/1—2014/12/31	38
	DE-Tha[b,e]	50.96	13.57	380	Germany	1996/1/1—2014/12/31	52
	US-Me2[b,e]	44.45	-121.56	1253	USA	2002/1/1—2014/12/31	43
	US-NR1[b,e]	40.03	-105.55	3050	USA	1998/1/1—2014/12/31	79
	AU-Cow[c]	-16.24	145.43	86	Australia	2010/1/1—2015/12/31	17
	AU-Ctr[c]	-16.10	145.45	66	Australia	2010/1/1—2017/12/31	8
Evergreen	US-SP3[a]	29.75	-82.16	50	USA	1999/1/1—2004/12/31	29
Broadleaf	AU-Rob[b,e]	-17.12	145.63	710	Australia	2014/1/1—12/31	9
Forest (EBF)	BR-Sa3[b,e]	-3.02	-54.97	100	Brazil	2000/1/1—2004/12/31	13
	AU-Wom[b,e]	-37.42	144.09	705	Australia	2010/1/1—2014/12/31	15
	FR-Pue[b,e]	43.74	3.60	270	France	2000/1/1—2014/12/31	37

	AU-Tum[b,e]	-35.66	148.15	1200	Australia	2001/1/1—2014/12/31	46
Deciduous Needle Forest (DNF)	FHK[d,e]	35.44	138.76	1100	Japan	2006/1/1—2013/12/31	17
	TMK[d,e,f]	42.74	141.52	140	Japan	2001/1/1—2004/12/31	13
Deciduous Broadleaf Forest (DBF)	AU-Lox[b,e]	-34.47	140.66	/	Australia	2008/1/1—2009/12/31	11
	IT-PT1[b,e]	45.20	9.06	60	Italy	2002/1/1—2004/12/31	12
	CA-TPD[b,e]	42.64	-80.56	260	Canada	2012/1/1—2014/12/31	12
	DK-Sor[b,e]	55.49	11.64	40	Denmark	1996/1/1—2014/12/31	10
	IT-Ro2[b,e]	42.39	11.92	160	Italy	2002/1/1—2012/12/31	20
	IT-Col[b,e]	41.85	13.59	1560	Italy	1996/1/1—2014/12/31	16
	DE-Hai[b,e]	51.08	10.45	430	Germany	2000/1/1—2012/12/31	27
	US-MOz[a]	38.74	-92.20	219	USA	2005/1/1—2006/12/31	13
	FR-Hes[a]	48.67	7.07	/	France	1997/1/1—2006/12/31	40
Mixed Forest (MF)	US-Syv[b,e]	46.24	-89.35	540	USA	2001/1/1—2014/12/31	21
	CA-Gro[b,e]	48.22	-82.16	340	Canada	2003/1/1—2014/12/31	21
	BE-Vie[b,e]	50.30	6.00	493	Belgium	1996/1/1—2014/12/31	17
	TSE[d,e]	45.06	142.11	70	Japan	2001/8/1—2002/12/31; 2004/1/1—2012/12/31	27
	GDK[d,e]	37.75	127.15	252	Korea	2004/1/1—2008/12/31	10
Closed Shrubland (CSH)	US-KS2[b,e]	28.61	-80.67	3	USA	2003/1/1—2006/12/31	18
	IT-Noe[b,e]	40.61	8.15	25	Italy	2004/1/1—2014/12/31	25
Open Shrubland (OSH)	CA-SF3[b,e]	54.09	-106.01	540	Canada	2001/1/1—2006/12/31	17
	ES-Amo[b,e]	36.83	-2.25	1200	Espain	2007/1/1—2012/12/31	34
Woody Savannah (WSA)	AU-RDF[b,e]	-14.56	132.48	171	Australia	2011/1/1—2013/12/31	15
	US-Ton[b,e]	38.43	-120.97	177	USA	2001/1/1—2014/12/31	57
Savannah (SAV)	BW-Ma1[a]	-19.92	23.56	~930	Botswana	2000/1/1—12/31	13
	ES-LMa[a]	39.94	-5.77	265	Spain	2004/1/1—2006/12/31	18
	SD-Dem[b,e]	13.28	30.48	500	Sudan	2005/1/1—2009/12/31	16

	AU-Dry[b,e]	-15.26	132.37	180	Australia	2008/1/1—2014/12/31	20
	AU-DaS[b,e]	-14.16	131.39	53	Australia	2008/1/1—2014/12/31	29
	AU-Cpr[b,e]	-34.00	140.59	53	Australia	2010/1/1—2014/12/31	36
	AU-Sam[c]	-27.39	152.88	87	Australia	2011/1/1—2017/12/31	45
	US-Aud[a]	31.59	-110.51	1469	USA	2003/1/1—2005/12/31	25
	PT-Mi2[a]	38.48	-8.02	~240	Portugal	2005/1/1—2006/12/31	10
	ES-VDA[a]	42.15	1.45	/	Spain	2004/1/1—2004/12/31	10
	HU-Bug[a]	46.69	19.60	/	Hungary	2003/1/1—2006/12/31	14
	US-FPe[a]	48.31	-105.10	634	USA	2000/1/1—2006/12/31	34
	CN-Du2[b,e]	42.05	116.28	/	China	2006/1/1—2008/12/31	12
	CN-Du3[b,e]	42.06	116.28	/	China	2009/1/1—2010/12/31	12
	RU-Ha1[b,e]	54.73	90.00	446	Russia	2002/1/1—2004/12/31	13
	US-ARb[b,e]	35.55	-98.04	424	USA	2005/1/1—2006/12/31	16
	US-ARc[b,e]	35.55	-98.04	424	USA	2005/1/1—2006/12/31	16
	CN-HaM[b,e]	37.37	101.18	/	China	2002/1/1—2004/12/31	15
	IT-Tor[b,e]	45.84	7.58	2160	Italy	2008/1/1—2014/12/31	23
Grassland	US-LWW[b,e]	34.96	-97.98	365	USA	1997/1/1—1998/12/31	19
(GRA)	AT-Neu[b,e]	47.12	11.32	970	Austria	2002/1/1—2012/12/31	13
	AU-TTE[b,e]	-22.29	133.64	553	Australia	2012/1/1—2014/12/31	18
	AU-Rig[b,e]	-36.65	145.58	162	Australia	2011/1/1—2014/12/31	17
	AU-Emr[b,e]	-23.86	148.47	/	Australia	2011/1/1—2013/12/31	23
	US-AR2[b,e]	36.64	-99.60	646	USA	2009/1/1—2012/12/31	27
	CN-Cng[b,e]	44.59	123.51	/	China	2007/1/1—2010/12/31	20
	US-Goo[b,e]	34.25	-89.87	87	USA	2002/1/1—2006/12/31	32
	US-AR1[b,e]	36.43	-99.42	611	USA	2009/1/1—2012/12/31	31
	DE-Gri[b,e]	50.95	13.51	385	Germany	2004/1/1—2014/12/31	37
	AU-Stp[b,e]	-17.15	133.35	225	Australia	2008/1/1—2014/12/31	39
	US-SRG[b,e]	31.79	-110.83	1291	USA	2008/1/1—2014/12/31	70
	US-Wkg[b,e]	31.74	-109.94	1531	USA	2004/1/1—2014/12/31	80
	US-Var[b,e]	38.41	-120.95	129	USA	2000/1/1—2014/12/31	126
Cropland	US-Bo1[a]	40.01	-88.29	219	USA	1997/1/1—2006/12/31	73

(CRO)	IT-CA2[b,e]	42.38	12.03	200	Italy	2011/1/1—2014/12/31	11
	US-CRT[b,e]	41.63	-83.35	180	USA	2011/1/1—2013/12/31	13
	US-Twt[b,e]	38.11	-121.65	-7	USA	2009/1/1—2014/12/31	10
	BE-Lon[b,e]	50.55	4.75	167	Belgium	2004/1/1—2014/12/31	13
	DE-Kli[b,e]	50.89	13.52	478	Germany	2004/1/1—2014/12/31	19
	FR-Gri[b,e]	48.84	1.95	125	France	2004/1/1—2014/12/31	9
	US-ARM[b,e]	36.61	-97.49	314	USA	2003/1/1—2012/12/31	46
	DE-Geb[b,e]	51.10	10.91	162	Germany	2001/1/1—2014/12/31	56
	US-Ne1[b,e]	41.17	-96.48	361	USA	2001/1/1—2013/12/31	87
	US-Ne2[b,e]	41.16	-96.47	362	USA	2001/1/1—2013/12/31	95
	US-Ne3[b,e]	41.18	-96.44	363	USA	2001/1/1—2013/12/31	92
	MSE[d,e]	36.05	140.03	13	Japan	2001/1/1—2006/12/31	22

Note: [a], [b], [c] and [d] represent that the sites are from LaThuile (https://fluxnet.org/data/la-thuile-dataset/), FLUXNET2015 Tier-2 (http://fluxnet.fluxdata.org/data/fluxnet2015-dataset/), OzFlux (https://data.ozflux.org.au/portal/home.jspx), and AsiaFlux (http://asiaflux.net/?page_id=23), respectively. [e] ([f]) suggests that LAI (CO_2 concentration) is not measured at this site and the GLASS LAI product (CO_2 concentration at Mauna Loa) will be used instead.

Table S2: Typical height for the 5 CSCS-based GRA groups

CSCS-based GRA group	Height (m)	Sources or references of the used EC sites
Tundra and alpine steppe GRA	0.32	CN-HaM[a], GL-ZaH[a], QHB[b], and DK-ZaH[a]
Semi desert GRA	0.39	Shapotou[c], CN-Sw2[a], Xiziwang Banner[c], US-Cop[a], AU-Ync[a], US-SRG[a], US-Aud[d], and AU-Sam[e]
Savanna	0.78	US-Wkg[d], AU-Emr[a], AU-Stp[a], AU-DaP[a]
Steppe GRA	0.28	US-FPe[d], KBU[b], AU-Rig[a], US-AR1[d], US-AR2[d], US-Var[d], PT-Mi2[a]
Temperate zonal humid GRA	0.43	Inner Mongolia[c], Xilinhot[c], CN-Du3[a], DK-Eng[a], IT-MBo, CN-Du2[a], DK-Lva[a], US-Bkg[d], Duolun[c], Hulun Buir[c]
Temperate zonal forest steppe GRA	0.52	CN-Cng[a], HU-Bug[a], LSH[b], YCS[b], Ansai[b], AT-Neu[a], CN-Dan[a], IT-Tor[a], RU-Ha1[a], SE-Deg[a], HBG[b], Arou[e], CH-Cha[a], CH-Fru[a], CH-Oe1[a], CZ-BK2[a], DE-RuR[a], DE-Gri[a], FR-Lq1[a], FR-Lq2[a], IT-Mala, ES-VDA[a], IE-Dria, NL-Hor[a], US-IB2[a], IT-Amp[a], and NL-Ca1[a]
Sub-tropical zonal forest steppe GRA	0.46	US-Arb[d], US-Arc[d], US-LWW[d], AU-Sam[a], US-Goo[d], and HFK[b]
Frigid desert GRA	0.33	Yin et al., (2019)
Warm desert GRA	0.50	White (1983), Suttie et al. (2005), Kadeba et al. (2015)
Tropical zonal forest steppe GRA	0.60	Prakash et al., (2020)

Note: [a], [b], [c] and [d] represent that the sites are from FLUXNET (http://fluxnet.fluxdata.org/), AsiaFlux (http://asiaflux.net/), ChinaFLUX (http://www.chinaflux.org/), AmeriFlux (https://ameriflux.lbl.gov/), HiWATER (https://data.tpdc.ac.cn/zh-hans/special/heihe/), and OzFlux (https://data.ozflux.org.au/portal/home.jspx), respectively.

Table S3: Cropland height (Allen et al., 1998)

Cropland types	Height (m)	Cropland types	Height (m)	Cropland types	Height (m)
Arabica coffee	2.50	Other fibre crops	1.35	Small millet	1.50
Banana	3.50	Oilpalm	8.00	Sorghum	2.25
Barley	1.00	Other oil crops	0.55	Soybean	0.75
Bean	0.40	Other pulses	0.80	Sugarbeet	0.45
Cassava	1.25	Other roots	0.50	Sugarcane	3.00
Chickpea	0.40	Pigeonpea	0.50	Sunflower	2.00
Coconut	8.00	Plantain	5.00	Sweet potato	0.40
Cocoa	3.00	Pearl millet	2.00	Tea	1.75
Cotton	1.35	Potato	0.60	Temperate fruit	3.92
Cowpea	0.40	Rapeseed	0.60	Tobacco	1.35
Groundnut	0.40	Robusta coffee	6.00	Tropical fruit	0.90
Lentil	0.50	Rest of crops	0.98	Vegetables	0.43
Maize	1.75	Rice	1.00	Wheat	1.00
Other cereals	1.00	Sesameseed	1.00	Yams	1.60

Table S4: w, z_{0g} and α_m values for various LULC types

LULC types	CRO	FR	GRA	SHRB	Tundra	Barren land	Snow/Ice
w_{max}[a] (m)	0.01	0.034	0.01	0.01	0.01	/	/
z_{0g}[a] (m)	0.005	0.02	0.01	0.02	0.01	0.001	0.001
α_m[a] (unitless)	0.20	0.17	0.23	0.18	0.23	0.15	0.70
$\Delta g_{1,CO2}$[b] (%)	0.36	0.23	0.25	0.40	0.36	/	/

Note: [a] represents this parameter is from Zhou et al. (2006), while [b] indicates that this parameter from Morison and Gifford (1984); Field et al. (1995); Saxe et al. (1998), Neitsch et al. (2002), Eckhardt and Ulbrich (2003), and Wu et al. (2017).

Table S5: The calibrated values of r_{smin} for each GLASS-GLC type

GLASS-GLC types	r_{smin} (s/m)
CRO	49.97
FR	105.97
GRA	112.89
SHRB	105.14
Tundra	80.00[a]
Barren land	120.00[a]
Snow/Ice	0[a]

Note: [a] represents that r_{min} is from Zhou et al. (2006).

References

Allen, R., Pereira, L., Raes, D. and Smith, M.: Crop Evapotranspiration Guidelines for Computing Crop Water Requirements. FAO Irrigation and Drainage Paper 56. Rome: Food and Agriculture Organization of the United Nations, 1998.

Brisson, N., Itier, B., L'Hotel, J. C. and Lorendeau, J. Y.: Parameterisation of the Shuttleworth-Wallace model to estimate daily maximum transpiration for use in crop models. Ecological Modelling, 107, 159–169, 1998.

Choudhury, B. J. and Monteith, J. L.: A four-layer model for the heat budget of homogeneous land surfaces. Quarterly Journal of the Royal Meteorological Society, 114, 373–398, 1988.

Dai, Y., Wei, N., Yuan, H., Zhang, S., Shangguan, W., Liu, S., Lu, X. and Xin, Y.: Evaluation of soil thermal conductivity schemes for use in land surface modelling. Journal of Advances in Modeling Earth Systems, 11(11), 3454–3473, 2019a.

Dai, Y., Xin, Q., Wei, N., Zhang, Y., Shangguan, W., Yuan, H., Zhang, S., Liu, S. and Lu, X.: (2019b), A global high-resolution dataset of soil hydraulic and thermal properties for land surface modeling. Journal of Advances in Modeling Earth Systems, 11(9), 2996−3023, 2019b.

Eckhardt, K. and Ulbrich, U.: Potential impacts of climate change on groundwater recharge and streamflow in a central European low mountain range. Journal of Hydrology, 284(1−4), 244−252, 2003.

Federer, C. A., Vorosmarty, C. J. and Fekete, B.: Intercomparison of methods for potential evapotranspiration in regional or global water balance models. Water Resources Research, 32, 2315–2321, 1996.

Field, C. B., Jackson, R. B. and Mooney, H. A.: Stomatal responses to increased CO_2: implications from the plant to the global scale. Plant, Cell & Environment, 18(10), 1214−1225, 1995.

Kadeba, A., Nacoulma, B. M. I., Ouédraogo, A., Bachmann, Y., Thiombiano, A., Schmidt, M. and Boussim, I. J.: Land cover change and plants diversity in the Sahel: a case study from northern Burkina Faso. Annals of Forest Research, 58(1), 109–123, 2015.

Monteith, J. L.: Principles of Environmental Physics. Edward Arnold, London, pp. 214, 1973.

Morison, J. I. L. and Gifford, R. M.: Plant growth and water use with limited water supply in high CO_2 concentrations. I. Leaf area, water use and transpiration. Functional Plant Biology, 11(5), 361−374, 1984.

Neitsch, S. L., Arnold, J. G., Kiniry, J. R., Williams, J. R. and King, K. W.: Soil and Water Assessment Tool Theo-retical Documentation, Version 2000. Soil and Water Research Laboratory and Blackland Research Center, Grassland, 2002.

Prakash, V., Bera, T., Pradhan, S. and Acharya, S. K.: Potential of *Syngonanthus nitens* fiber as a reinforcement in epoxy composite and its mechanical characterization. Journal of the Indian Academy of Wood Science, 17, 73–81, 2020.

Reddy, S. J.: An empirical method for estimating sunshine from total cloud amount. Solar Energy, 15(4), 281–285, 1974.

Saxe, H., Ellsworth, D. and Heath, J.: Tree and forest functioning in an enriched CO_2 atmosphere. New Phytologist, 139(3), 395−436, 1998.

Shuttleworth, W. J.: Evaporation. In: Maidment, D. R. (Ed.), Handbook of Hydrology. McGraw-Hill, New York, pp. 4.1–4.53, 1993.

Shuttleworth, W. J. and Wallace, J. S.: Evaporation from sparse crops – an energy combination theory. Quarterly Journal of the Royal Meteorological Society, 111, 839–855, 1985.

Shuttleworth, W. J. and Gurney, R. J.: The theoretical relationship between foliage temperature and canopy resistance in sparse crops. Quarterly Journal of the Royal Meteorological Society, 116, 497–519, 1990.

Suttie, J. M., Reynolds, S. G. and Batello, C.: Grasslands of the World. Plant Production and Protection Series No. 34. Rome: Food and Agriculture Organization of the United Nations, 2005.

Uchijima, Z.: Maize and rice. In: Monteith, J. L. (Ed.), Vegetation and the Atmosphere, vol. 2. Academic Press, New York, pp. 33–64, 1976.

Villagarcía, L., Were, A., Garcíac, M. and Domingo, F.: Sensitivity of a clumped model of evapotranspiration to surface resistance parameterizations: Application in a semi-arid environment. Agricultural and Forest Meteorology, 150, 1065–1078, 2010.

White, F.: The vegetation of Africa. Paris: UNESCO, 1983

Wu, L., Min, L. L., Shen, Y. J., Zhou, X. X. and Liu, F. G.: Simulation of maize evapotranspiration at different growth stages using revised dual-layered model in arid Northwest China. Chinese Journal of Eco-Agriculture, 25(5), 634−646, 2017. (in Chinese with English Abstract)

Yin, J., Feng, Q., Liang, T., Meng, B., Yang, S., Gao, J., Ge, J., Hou, M., Liu, J., Wang, W., Yu, H. and Liu, B: Estimation of grassland height based on the random forest algorithm and remote sensing in the Tibetan Plateau. IEEE Journal of Selected Topics in Applied Earth Observations and Remote Sensing, 13, 178–186, 2019.

Zhang, B., Kang, S., Li, F. and Zhang, L.: Comparison of three evapotranspiration models to Bowen ratio-energy balance method for a vineyard in an arid desert region of northwest China. Agricultural and Forest Meteorology, 148(10), 1629−1640, 2008.

Zhou, M. C., Ishidaira, H., Hapuarachchi, H. P., Magome, J., Kiem, A. S. and Takeuchi, K.: Estimating potential evapotranspiration using Shuttleworth-Wallace model and NOAA-AVHRR NDVI data to feed a distributed hydrological model over the Mekong River basin. Journal of Hydrology, 327, 151–173, 2006.